11-2009

How Does The Relocation Of Internal Water Affect Resonance Raman Spectra Of Rhodopsin? An Insight From Casscf/amber Calculations

Tadeusz Andruniow

Massimo Olivucci
Bowling Green State University, molivuc@bgsu.edu

JCTC Journal of Chemical Theory and Computation

How Does the Relocation of Internal Water Affect Resonance Raman Spectra of Rhodopsin? An Insight from CASSCF/Amber Calculations

Tadeusz Andruniów*,† and Massimo Olivucci‡,§

Quantum Chemistry and Molecular Modelling Lab, Institute of Physical and Theoretical Chemistry, Wroclaw University of Technology, Wyb. Wyspianskiego 27, 50-370 Wroclaw, Poland, Dipartimento di Chimica, Università di Siena, via Aldo Moro 2, 53100 Siena, Italy, and Chemistry Department, Bowling Green State University, Bowling Green, Ohio 43403

Received February 9, 2009

Abstract: The effect of relocation of the W2 crystallographic water in bovine rhodopsin has been investigated by comparing and analyzing simulated resonance Raman spectra of 1HZX- and 1U19-based quantum mechanics/molecular mechanics (CASSCF/MM) models. The main target is to explore the sensitivity of the simulated resonance Raman spectra to protein cavity change. In particular, we focus on a quantitative investigation of the changes in the vibrational activity of rhodopsin induced by modifications in the protein cavity structure and in the water position. Comparison of the simulated RR spectra of the *Rh-1U19* and *Rh-1HZX* models with the measured spectrum of rhodopsin reveals that the *Rh-1U19* model provides a slightly better rhodopsin model consistently with the simulations of the absorption maxima. On the other hand, and irrespective of the comparison with the experimental data, the analysis of two different computational models for the same protein and chromophore makes it possible to investigate and disentangle the relationship between structural features and change in the RR intensities in an unusually detailed way.

Introduction

The visual pigment rhodopsin is a G protein-coupled receptor responsible for dim-light vision in vertabrates. Rhodopsin contains an 11-*cis* retinal chromophore bound to a lysine residue via a protonated Schiff base linkage (PSB11). The biological activity of rhodopsin is triggered by the ultrafast light-induced *cis*−*trans* isomerization of the chromophore that initiates the vision process. The isomerization reaction is very efficient and extremely fast - the chromophore isomerizes to the *all-trans* photoproduct within a few picoseconds and with a quantum yield of 0.67.[1]

Since Palczewski and co-workers reported the first X-ray crystal structure of bovine rhodopsin at 2.8 Å resolution (1F88), there has been an ever increasing interest in diffraction studies on rhodopsin. Indeed, a year later, an improved model (1HZX) from the same groups[3] revealed some missing residues from the original structure. 1HZX contains only one internal water molecule (W1), positioned between PSB11 and the Glu181 residue. Soon after, two additional crystallographic structures, resolved at 2.6[4] and 2.2 Å[5] (1L9H and 1U19, respectively), were deposited in the ProteinDataBank archive. The 1HZX location of W1 is retained in 1L9H and 1U19. However, both 1L9H and 1U19 report a newly identified water molecule (W2) placed close to PSB11 and the chromophore carboxylate counterion Glu113. It is believed that internal water molecules may have an important role in regulating the activity of rhodopsin.[4]

A recent computational study on bovine rhodopsin[6] has investigated the effect of relocation of the W2 crystallographic water by comparing and analyzing the vertical excitation energy of the 1HZX- and 1U19-based quantum

* Corresponding author e-mail: andruniow@mml.ch.pwr.wroc.pl.
† Wroclaw University of Technology.
‡ Università di Siena.
§ Bowling Green State University.

10.1021/ct900071c CCC: $40.75
Published on Web 10/13/2009

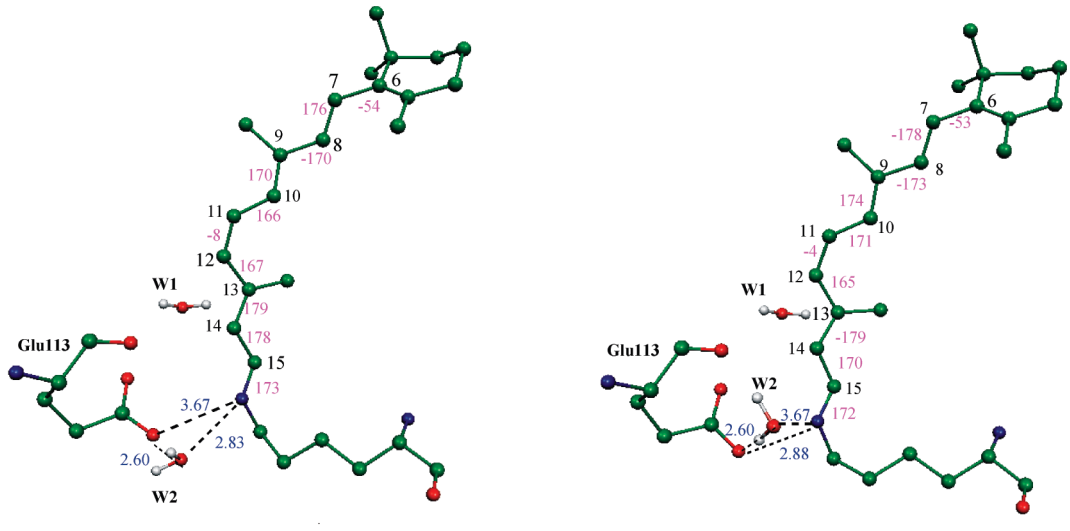

Figure 1. 11-*cis* retinal frameworks with Glu113 and W1 and W2 molecules. The ground-state optimized structure on the left corresponds to *Rh-1HZX*, while the structure on the right corresponds to *Rh-1U19*. Dihedral angles (in degrees) are indicated in pink. Some critical distances between W2 water and the Schiff base region and/or the counterion are in blue (in Å).

mechanics/molecular mechanics models (see Figure 1). Using CASSCF/Amber optimized structures of such models and subsequent single-point CASPT2//CASSCF/Amber computations the authors have been able to compute a red-shifting effect moving the absorption maximum from 479 nm (59.8 kcal·mol^{-1} vertical excitation energy) for the 1HZX-based model (*Rh-1HZX*) to 513 nm (55.7 kcal·mol^{-1} vertical excitation energy) for the 1U19-based model (*Rh-1U19*). Since the observed absorption maximum is 498 nm (57.4 kcal· mol^{-1} vertical excitation energy) the 1U19-based model leads to a smaller −1.8 kcal·mol^{-1} red-shifted error. A comparative analysis of the two models reveals that the change in absorption maximum is not due to a single structural change such as W2 relocation but to simultaneous changes in the PSB11-counterion distance and to a substantial PSB11 chain displacement within the (modestly) different protein cavity structures.

Resonance Raman (RR) spectroscopy is a powerful experimental technique for probing the structural changes of chromophores. In fact, even limited changes in the chromophore structure, or in the relationship of the chromophore with its environment, usually result in clear changes in the spectrum vibrational pattern and intensities. RR spectra are generated via electronic excitation in the Franck−Condon vicinity and display the intensity of vibrational modes coupled to the electronic transition. Moreover, RR spectra provide detailed information on the difference of the ground and excited state molecular structures of the chromphore as well as on its initial excited state dynamics. In the past, the RR studies of the PSB11 retinal chromophore of rhodopsin were very useful in identifying the photoreaction intermediates and the initial excited-state dynamics of the photoisomerization process.[1] In these studies the effect of the protein environment was scrutinized by comparing the RR spectra of PSB11 in solution and in the protein.[7−9]

In this article we report simulations of RR spectra of rhodopsin for *Rh-1HZX* and *Rh-1U19* models (Figure 1) using the CASSCF/Amber method to calculate the ground state force field. The main target is to explore the sensitivity of the simulated RR spectra to protein cavity changes. In particular, we focus on a quantitative investigation of the changes in the vibrational activity of rhodopsin induced by modifications in the protein cavity structure and in the water position. A comparison of the simulated RR spectra of *Rh-1U19* and *Rh-1HZX* models reveals that there are non negligible differences in vibrational frequencies and intensity distribution in both spectra. The results also show that the *Rh-1U19* model allows for a slightly more detailed reproduction of the experimental RR spectrum consistently with the simulations of the absorption maxima. On the other hand, and irrespective of the comparison with the experimental data, the analysis of two different computational models for the same protein and chromophore makes it possible to investigate and disentangle the relationship between structural features and change in the RR intensities in an unusually detailed way.

Models and Methods

The first model (*Rh-1HZX*) investigated in this study is based on monomer A of 1HZX crystal structure. In addition to one internal water molecule present in the original protein structure, the second internal water molecule was introduced following a suggestion by Kandori et al.[10] This model was utilized in our early studies on rhodopsin.[11−13] The second model (*Rh-1U19*) was prepared, using the same procedures, from 1U19 crystal structure that comprises two resolved water molecules close to the chromophore binding site. As displayed in Figure 2, the position of W2 in *Rh-1U19* differs significantly from that seen in *Rh-1HZX*. Even though W2 is invariably hydrogen-bonded to the O1 carboxylate oxygen of Glu113 counterion in both structures, its position is strongly shifted to the opposite side of Glu113 in *Rh-1U19* relative to *Rh-1HZX* models.

The retinal chromophore bears a net positive charge counterbalanced by a negative charge of Glu113 residue. The

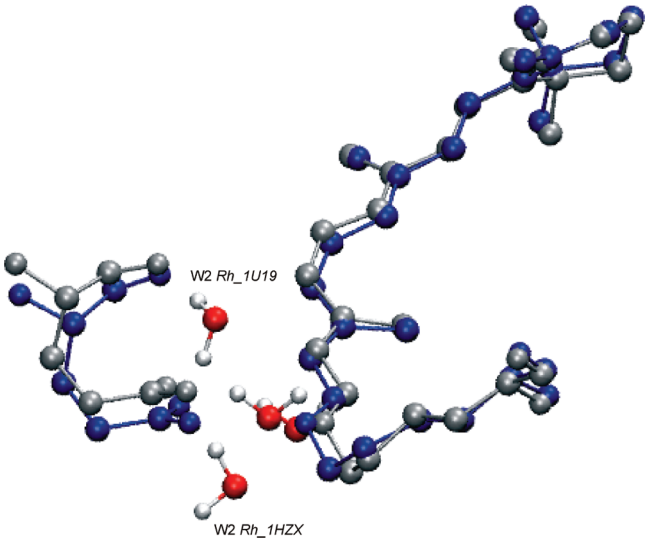

Figure 2. Superposition of the ground-state optimized *Rh-1HZX* (in silver) and *Rh-1U19* (in blue) 11-*cis* retinal chromophores. Notice a different orientation of the W2 molecule in both rhodopsin models.

rest of the protein cavity is set to neutral. Even though there is conflicting evidence in the literature regarding the protonation state of Glu181 residue,[14−20] a recent study by Hall et al.[21] has shown that changing the protonation state of Glu181 has a rather minimal effect on properties of PSB11 in rhodopsin. The average equilibrium structure of the rhodopsin models is generated via geometry optimization by relaxing the chromophore, Lys296 residue, and the two TIP3P-type water molecules, while the rest of the protein is kept frozen in its X-ray position during optimization procedure. Such a fixed structure is taken as representative of the average protein environment. With the exception of Lys296, the residue charges are described by the standard Amber force field.[22]

Recently we have shown that CASPT2//CASSCF/MM calculations provide a quantitative evaluation of structural and spectroscopic parameters for rhodopsin,[11−13] GFP,[23] and retinal-based molecular switches.[24,25] Also, previous CASSCF/Amber studies on the RR spectrum of *Rh-1HZX*[13] showed a relatively good agreement with the experimental spectrum.[8] However, a modest basis set (3-21g*) used in these studies resulted in significant blueshift of the most intense band in the calculated spectrum with respect to the measured one.[8] Therefore, in our present CASSCF simulations of the *Rh-1HZX* RR spectrum we have employed a more extensive basis set (6-31g*) than before.[13] Additionally, it should be pointed out that the RR spectrum of *Rh-1U19* has been simulated for the first time. The effect of isotopic substitution and normal mode composition analysis was done to aid in the assignment of experimental bands. The wavenumber shifts were calculated upon C_{10}-D, C_{14}-D, 10,11-^{13}C, 14,15-^{13}C, and N-D substitution and compared with those measured previously[7] in RR experiments. Potential energy distribution (PED) contribution to each of the calculated vibrational frequency gives insight into the normal mode composition which in turn aids in the assignment of the measured resonance Raman bands. Veda4[26] software was used to perform PED analysis.

We have calculated Raman intensities under resonant conditions applying a sum-over-states formalism developed by Albrecht[27] where the transition polarizibility tensor is written as

$$\alpha_{fi}^{\rho\sigma}(\Omega) = \sum_{e}\sum_{v}\left[\frac{\langle f|\mu_{ge}^{\rho}|k\rangle\langle k|\mu_{eg}^{\sigma}|i\rangle}{E_{ek} - E_{gi} - \Omega + i\Gamma_{ek}} + \frac{\langle f|\mu_{ge}^{\sigma}|k\rangle\langle k|\mu_{eg}^{\rho}|i\rangle}{E_{ek} - E_{gf} + \Omega + i\Gamma_{ek}}\right] \quad (1)$$

In eq 1 the sum runs over all electronic $|e\rangle$ and vibrational $|v\rangle$ states, $|i\rangle$ and $|f\rangle$ are initial and final vibrational states, respectively, of the electronic ground state, while $|k\rangle$ is an intermediate vibrational state of the electronic excited state, Ω is the frequency of the incident light, E_{gi}, E_{ek}, and E_{gf} are vibronic energies of initial, intermediate and final states, Γ_{ek} is a damping factor associated with the g→e electronic transition, and $\mu_{ge/eg}^{\rho/\sigma}$ is the electronic transition dipole moment.

Upon expanding the transition dipole moments in the Taylor series in terms of the molecular normal modes and ignoring the vibronic coupling effects, the Franck−Condon (FC) mechanism can be described by the following expression

$$\alpha_{fi}^{\rho\sigma}(\Omega) = \sum_{e}\mu_{ge}^{\rho 0}\mu_{eg}^{\sigma 0}\sum_{v}\left[\frac{\langle f|k\rangle\langle k|i\rangle}{E_{ek} - E_{gi} - \Omega + i\Gamma_{ek}} + \frac{\langle f|k\rangle\langle k|i\rangle}{E_{ek} - E_{gf} + \Omega + i\Gamma_{ek}}\right] \quad (2)$$

If only one electronic excited state contributes to the Raman scattering eq 2 simplifies to

$$\alpha_{fi}^{\rho\sigma}(\Omega) = \sum_{e}\mu_{ge}^{\rho 0}\mu_{eg}^{\sigma 0}\sum_{v}\left[\frac{\langle f|k\rangle\langle k|i\rangle}{E_{ek} - E_{gi} - \Omega + i\Gamma_{ek}}\right] \quad (3)$$

where $\mu_{ge/eg}^{\rho 0/\sigma 0}$ is a pure electronic transition dipole moment.

By adapting harmonic approximation and identical vibrational frequencies and normal coordinates in the ground and excited electronic states it is possible to calculate the FC overlap from recursion formulas given in ref 28. Subsequently, the square of the transition polarizibility is proportional to the dimensionless parameter B_k through the relation[29]

$$|(\alpha_{fi}^{\rho\sigma}(\Omega))_k|^2 \propto \frac{B_k^2}{2} \quad (4)$$

and this in turn is related to the RR intensity of the kth vibration

$$I_k \propto \frac{B_k^2}{2} \quad (5)$$

Dimensionless displacements B_k of the potential energy surface minima along the k totally symmetric vibrational modes are defined as[29−31]

$$B_k = S_k^T \Delta X \left(\frac{\mu_k \omega_k}{\hbar}\right)^{1/2} \quad (6)$$

where S_k is a 3N-dimensional vector containing the Cartesian nuclear displacements in Q_k normal mode with the associated

frequency ω_k and reduced mass μ_k. ΔX is the 3N-dimensional vector containing the differences of the nuclear position vectors in the resonant and ground electronic states.[30,31]

There have been successful attempts to calculate RR spectra using Kramers−Kronig transform procedure which eliminates the need for explicit summation over intermediate vibrational levels.[32−36] An alternative to the sum-over-states formulation is the Heller's time-dependent approach.[37−39] In the "short-time" limit of the time-dependent approach[36,37] which applies to preresonance conditions or fast electronic relaxation the relative intensities are given by

$$I_k = \omega_k^2 B_k^2 \tag{7}$$

where ω_k is the frequency of the kth vibration and dimensionless parameters B_k are calculated from the excited-state gradients. Thus, within this approximation no explicit knowledge of the excited-state equilibrium structure is required.

Based on eqs 5 and 7 it is clear that to evaluate the resonance Raman intensities we need dimensionless parameters. These in turn can be calculated having the equilibrium geometries of the ground state and the excited state (or excited-state gradient at the ground state equilibrium geometry) in resonance with the excitation wavelength as well as the vibrational frequencies at the ground state equilibrium geometry.

The QM/MM employed in this study is fully described in ref 11. In short, the QM subsystem consists of retinal and the last bond of Lys296 side chain. We use a hydrogen link-atom scheme with the frontier placed at the C_ε-C_δ bond of the Lys296. The *ab initio* calculations are based on the CASSCF level of theory. In the optimization step the 6-31G* basis set was used, while the 3-21G* basis set was chosen to obtain second-derivatives. In the geometry optimization procedure the active space comprises the full π-system of PSB11 (12 electrons in 12 π-orbitals), which is reduced to 8 electrons in 8 orbitals during the frequency calculations. Accordingly, in the latter the 2 lowest occupied and 2 highest unoccupied retinal π-orbitals were excluded from the active space. CASSCF/MM geometry optimization of the ground state and optically allowed excited state rhodopsin structures as well as frequency calculations in the ground state were carried out with the programs Gaussian03[40] and Tinker.[41]

In calculations of resonance Raman intensities for *Rh-1U19* we used the sum-over-states approach described by eq 3. Since eq 5 is often employed in simple estimation of RR intensities of large molecules we compared a spectrum resulting from eq 5 with the more accurate one obtained from eq 3. Furthermore, the "short-time" approximation is also applied to model Raman spectrum of *Rh-1U19*. We examined some possible approximations originating from the sum-over-states as well as from the "short-time" approaches by comparing the resulting simulated RR spectra to each other and to the experimental spectrum. Notice that eq 3 provides the possibility of calculating RR intensities not only for fundamentals but also for overtones and combination bands; however, it significantly increases the computational effort. On the other hand, the two other methods described above are much more efficient but can only be used to obtain intensities of fundamentals.

The qualitative difference between simplified sum-over-states and "short-time" approaches is illustrated in Figure S1 (Supporting Information). Spectra A and B obtained with the use of sum-over-states relations (eqs 3 and 5, respectively) combined with B_k calculated from the shift between the excited state and ground state equilibrium positions reveal very similar intensity distribution. It is interesting to note that fundamentals and overtones do not manifest themselves in the 700−1750 cm^{-1} frequency region of spectrum A (Figure S1 (Supporting Information)). On the other hand, comparison of spectra A and B with the spectrum determined from the "short-time" approximation (spectrum C) based on the excited state gradient's B_k reveals subtle changes in the intensity pattern of the 900−1050 cm^{-1} frequency region, notably a band at around 940 cm^{-1} which is extremely weak in spectrum C, while in other theoretical and experimental spectra[8] it brings substantial intensity. Moreover, the intensity of the 1632 cm^{-1} band is exaggerated in comparison to its experimental counterpart. Overall, the simulated spectra originated from simplified approaches are amazingly similar to the spectrum obtained from more demanding the sum-over-states approach expressed by eq 3. In light of these findings we will use eq 5 to calculate RR spectra of *Rh-1U19* and *Rh-1HZX*.

To improve the agreement between calculated and experimental frequencies we used a scaling factor for CASSCF-based frequencies equal to 0.9 to account for errors due to incomplete treatment of dynamic electron correlation, basis set truncation, modest active space, and anharmonic effects. The spectra were obtained as superpositions of the Lorentzian curve with the line width of 10 cm^{-1}.

Results and Discussion

As discussed above, Strambi et al.[6] have analyzed the sensitivity of the absorption maxima of rhodopsin to the change in the crystallographic structure (mainly differing for the relocation of one of the internal water molecules). To do so, they have calculated the ground state equilibrium structures as well as the excitation energies for the *Rh-1HZX* and *Rh-1U19* models. Inspection of Figure 2 shows that the W1 position is hardly changed in the models. On the other hand, in *Rh-1HZX*, W2 forms a single hydrogen bond with the O1 carboxylate oxygen of Glu113 whereas, in *Rh-1U19*, W2 is hydrogen-bonded to both O1 and to the oxygen of the nearby peptide bond. It is interesting to note that a major relocation of W2 water molecule in *Rh-1U19* while leading to a large (0.7−0.8 Å) decrease in the -C=NH(+)----O1(-) salt-bridge distance—exposing the -C=NH(+) to a more negative electrostatic potential—does not dramatically affect the excitation energy.[6] This is explained with the relocation of the retinal chain shown in Figure 2 where we report a superimposed PSB11 structure in *Rh-1HZX* and *Rh-1U19*. Indeed the computed change in the cavity generated electrostatic potential[6] points to a compensation mechanism where the shifting of the -C=NH(+) chromophore position in *Rh-1U19* with respect to *Rh-1HZX* results in the exposure of such moiety to a more positive electrostatic potential that

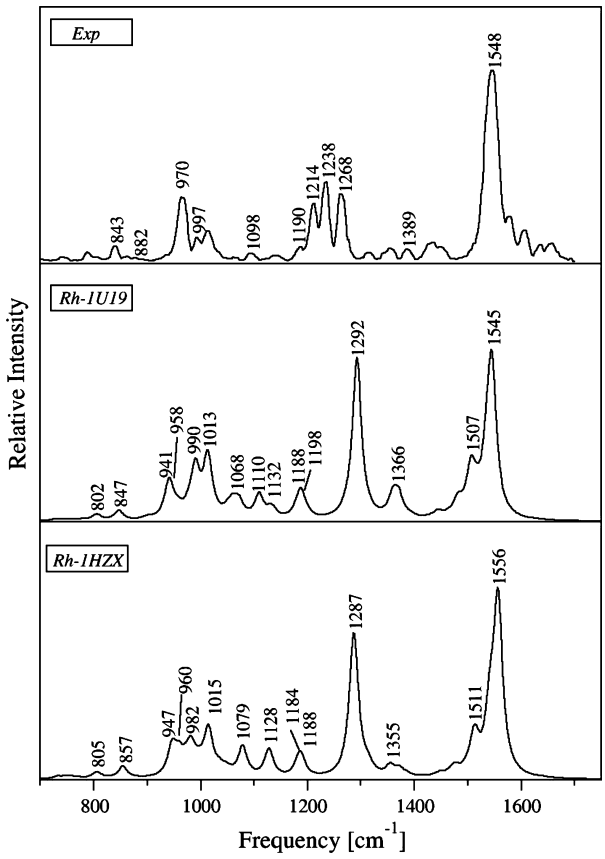

Figure 3. Simulated resonance Raman spectra for *Rh-1HZX* and *Rh-1U19* and their comparison with the experimental spectrum.[7]

overcompensates the effect of the closer O1 counterion negative charge. While such an effect is responsible for a ca. 4 kcal·mol^{-1} decrease in vertical excitation energy,[6] we want to determine if this effect is also accompanied by a change in the RR spectra of the corresponding models. In other words, a large change in hydrogen-bonding of the chromophore shall manifest itself in altered vibrational frequencies and/or intensities of specific vibrational modes and thus can be conveniently investigated by comparing the vibrational activity of RR spectra for both rhodopsin models.

The RR spectra of both models are reported in Figure 3 together with the observed spectrum. As it was shown by Mathies and co-workers the most characteristic parts of the resonance Raman spectrum of bovine rhodopsin are (1) the ethylenic band observed between 1500 and 1650 cm^{-1}, (2) the structurally sensitive fingerprint region observed in the 1100−1350 cm^{-1} frequency range, (3) the hydrogen out-of-plane (HOOP) region observed in the 900−1100 cm^{-1} frequency range, and (4) the low-frequency region comprising of torsional modes associated with the isomerization reaction.[8]

The high-frequency region of the *Rh-1HZX* model is qualitatively similar to that of *Rh-1U19* (Figure 3). There are two strong lines at 1556 and 1542 cm^{-1} in the former that correspond to peaks at 1545 and 1536 cm^{-1} in *Rh-1U19*. These intense lines are assigned to an in-phase stretching of the C11═C12 bond combined with the C9═C10 stretch. The ethylenic stretching frequency in *Rh-1U19* is shifted down by 11 cm^{-1} from the frequency in *Rh-1HZX*, and this is consistent with a red-shift of its absorption.[6] This frequency downshift also corresponds well to the increase in the C11═C12 and C9═C10 distances by 0.004 and 0.003 Å, respectively, going from *Rh-1HZX* to *Rh-1U19*. In the experiment[8] the lower-intense line was not detected, so it may be hidden under the fairly broad band at 1548 cm^{-1}. Consistently with *Rh-1HZX*, there is also a weaker line calculated on the left wing of the 1545 cm^{-1} band in *Rh-1U19*. This band is shifted by 6 cm^{-1} relative to the frequency in *Rh-1HZX* (1542 cm^{-1}) and is due to noticeable contribution from the C13═C14 stretch.

The frequency of the C═N stretching is considered to be a sensitive probe of the Schiff base-protein interactions in rhodopsin.[1] Strambi et al.[6] have demonstrated that relocation of one internal (W2) water molecule in *Rh-1U19* results in a strongly reduced C═NH(+)----O1(−) salt-bridge distance that must induce a decrease in double bond delocalization, an increase in vertical excitation energy, and a modified hydrogen-bond network. As explained above, such effects are more than counterbalanced by an effective PSB11 displacement to a region with a larger protein-generated positive potential that explains the calculated red-shift relative to the *Rh-1HZX* model. Indeed, the C═N stretching mode in *Rh-1HZX* was obtained at 1640 cm^{-1}, while in *Rh-1U19* at 1632 cm^{-1} and likely corresponds to the band at 1655 cm^{-1} in the measured spectrum.[8] However, it is interesting that the calculated frequency shift induced by N-deuteration, which is 42 cm^{-1} in *Rh-1U19*, drops to 24 cm^{-1} in *Rh-1HZX* (experimental shift is in a range of 31−35 cm^{-1})[7,49] implying much stronger coupling of the C═N stretch with the N−H bending vibration in *Rh-1U19*. The considerably lower frequency shift predicted for *Rh-1HZX* can be ascribed to the weakened Schiff base hydrogen bonding in the *Rh-1HZX* model, in accordance with recently calculated structural data.[6,12]

The frequencies of C−C stretches are sensitive to local geometry and thus provide valuable information on the conformation of retinal.[1,8] The fingerprint region is characterized by single-bond C−C stretching modes and spans 1100−1350 cm^{-1} spectral range. In the calculated resonance Raman spectra of both *Rh-1HZX* and *Rh-1U19* two modest bands are observed at 1188 and 1128 cm^{-1} in the former and 1198 and 1132 cm^{-1} in the latter (Figure 3 and Table 1). For *Rh-1HZX*, the 1188 cm^{-1} mode can be assigned to the C8−C9 stretch, while the 1184 cm^{-1} mode can be assigned to the C12−C13 stretch. The corresponding modes in *Rh-1U19* are upshifted by 10 and 4 cm^{-1}, respectively. A normal-mode analysis in this region is obscured by the fact that C−C stretches are strongly delocalized over the discussed fingerprint modes and thus difficult to assess in terms of local mode coordinates in agreement with previous DFT-based vibrational study.[43] However, the assignment was facilitated by calculating the positions of the fingerprint modes for the isotopically labeled analogues of *Rh-1HZX* and *Rh-1U19*. In fact, the C12−C13 stretch can be assigned with confidence at 1184 cm^{-1} in *Rh-1HZX* (1188 cm^{-1} in *Rh-1U19*) as only this line does exhibit the characteristic coupling with C14H bending, shifting up by 33 cm^{-1} in C14D derivative (38 cm^{-1} in *Rh-1U19*). Similarly, the 1188 cm^{-1} mode in *Rh-1HZX* (1198 cm^{-1} in *Rh-1U19*) can be characterized as the C8−C9 stretch based on the 33 cm^{-1} (32

Table 1. Selected Calculated Normal Mode Frequencies (cm^{-1}) and Relative Intensities of the PSB11 Chromophore of Rhodopsin *Rh-1HZX* and *Rh-1U19* Models[c]

	Rh-1HZX		*Rh-1U19*		experiment	
assignment	freq	I/I_{1556}[a]	freq	I/I_{1545}[a]	freq	I/I_{1548}
C=N stretch	1640	0.004	1632	0.002	1655	0.069
in-phase C=C stretch	1556	1.000	1545	1.000	1548	1.000
C8−C9 stretch	1188	0.096	1198	0.023	1214	0.210
C12−C13 stretch	1184	0.075	1188	0.179	1238	0.250
C14−C15 stretch	1128	0.173	1132	0.074	1190	0.029
C10−C11 stretch	1058	0.004	1055	<0.001	1098	0.026
C11=C12 A_2 HOOP - C11=C12 torsion	982	0.153	990	0.327	970	0.260
C7=C8 A_u HOOP + C7=C8 torsion	960	0.033	958	0.044	976	[b]
C10H wag - C7=C8 B_g HOOP	857	0.074	847	0.066	882	<0.01
C7=C8 B_g HOOP + C10H wag	805	0.036	802	0.020	843	0.040

[a] Resonance Raman intensity of a mode relative to the intensity of the ethylenic stretching mode (1556 cm^{-1} in *Rh-1HZX* and 1545 cm^{-1} in *Rh-1U19*). Intensities were calculated using eq 5. [b] No detectable scaterring intensity in the observed spectrum (ref 8). [c] Comparison with the experimental data from ref 8.

cm^{-1} in *Rh-1U19*) upshift upon C10D substitution. The C10−C11 stretch in *Rh-1HZX* is predominantly localized at the 1058 cm^{-1} mode on the basis of its 11 cm^{-1} downshift to 1047 cm^{-1} in 10,11-^{13}C derivative. Also, the same magnitude of the shift in the 10,11-^{13}C spectrum of *Rh-1U19* indicates that the 1055 cm^{-1} mode is of C10−C11 character. A very weak C10−C11 line seen in the experimental spectrum[8] at 1098 cm^{-1} does have a negligible intensity in the calculated spectra. In *Rh-1U19* contribution from the C14−C15 single bond can be found in numerous modes; however, the mode with the strongest intensity is located at 1132 cm^{-1}. This mode becomes even stronger in *Rh-1HZX*. The assignment of the C14−C15 stretch at 1128 cm^{-1} is strongly supported by the 24 cm^{-1} (22 cm^{-1} in *Rh-1U19*) isotopic shift in the 14,15-^{13}C derivative in good agreement with the 22 cm^{-1} experimental shift.[7] Nevertheless, the calculated C14−C15 stretching frequency in both *Rh-1HZX* and *Rh-1U19* is considerably lower than the measured value (ca. 60 cm^{-1})[8] reflecting the exaggerated contribution from C−C−H and C−N−H bending motions. A prominent band calculated at ca. 1290 cm^{-1} in both cavities can be attributed to the 1268 cm^{-1} 11H−12H rocking, totally symmetric motion. The intensity of this mode calculated for *Rh-1HZX* and *Rh-1U19* is too strong relative to the corresponding ethylenic band when compared to the experimental intensity pattern.[8]

The analysis of the vibrational activity applied to the 1100−1650 cm^{-1} region shows a dramatic intensity increase of the line assigned to the C14−C15 stretching mode as compared to the intensities of the C8−C9 and C12−C13 stretchings when going from *Rh-1U19* to *Rh-1HZX*. Although the calculated RR intensities of the bands ascribed to C8−C9, C12−C13, and C10−C11 stretchings are too weak in comparison to the measured values,[8] these data indicate that the intensity pattern of the fingerprint region in the RR spectrum of *Rh-1U19* reveals closer agreement with the observed spectrum. It is interesting to note that the frequencies of the corresponding C−C stretching modes decrease, while the frequency of the corresponding ethylenic mode increases in *Rh-1HZX* relative to *Rh-1U19*, thus reflecting more delocalized electronic structure of the red-absorbing *Rh-1U19* (Table 1).

In our studies we have selected a single scaling factor for all normal-mode frequencies; however, one may notice a rather interesting pattern—the frequencies of the C−C stretches are consistently 16−62 cm^{-1} downshifted relative to the experimental values. A rationale for the red-shifted C−C frequencies is the CASSCF tendency to lengthen the C−C single bonds in retinal backbone.[44] On the other hand, there is no anticipated blueshift of the in-phase C=C frequency in both rhodopsin models (3 cm^{-1} decrease in *Rh-1U19* and 8 cm^{-1} increase in *Rh-1HZX*) as compared to the observed value,[7] despite the fact that CASSCF-based C=C bonds are strongly strengthened in relation to experimental data.[5] However, the inclusion of a dynamic correlation energy through denisity functional theory (DFT) frequency calculations on the CASSCF-derived equilibrium structures of both rhodopsin models shifts the calculated frequency of the C11=C12 stretching mode above the measured value up to 1557 cm^{-1} in *Rh-1U19* and 1567 cm^{-1} in *Rh-1HZX*.[50] Moreover, reduced active space in the CASSCF calculations and consequently unbalanced electron correlation as well as modest basis set also have a large impact on the systematic deviation of the calculated frequencies and the measured ones. To refine C−C vibrational frequencies one would have to derive a set of scaling factors, but this is beyond the scope of the present work.

In contrast to the fingerprint modes, HOOP modes are highly localized, and their assignment becomes straightforward. Since the relative intensity of these modes is sensitive to structural perturbation it does provide information on protein-chromophore interactions in rhodopsin,[7,8] rhodopsin intermediates,[45−48] and other visual pigments.[42,49] The spectrum of *Rh-1HZX* is characterized by strong bands at 1015, 982, 960, and 947 cm^{-1} that have their counterparts in *Rh-1U19* spectrum at 1013, 990, 958, and 941 cm^{-1}. The bands at ca. 1130 cm^{-1} are assigned to methyl rocking vibrations. The calculations predict that the 990 cm^{-1} mode contains HOOP and torsional character of the C11=C12 bond. This mode was observed at 970 cm^{-1} in the experimental resonance Raman spectrum.[8] It shifts down by 8 cm^{-1} and decreases in intensity when going from *Rh-1U19* to *Rh-1HZX*. The normal mode calculated at ca. 960 cm^{-1} in both *Rh-1HZX* and *Rh-1U19* is a coupled vibration of the C7=C8 A_u HOOP and C7=C8 torsion. This HOOP mode was detected experimentally at 976 cm^{-1}.[8] It seems that *Rh-1HZX* provides slightly better correlation with the experimental data

concerning C11=C12 and C7=C8 HOOP frequencies. On the other hand, a rather strong C11=C12 HOOP peak in *Rh-1U19* closely mirrors the observed intensity (Table 1). There is yet another intense band in this region located at essentially the same frequency (941 cm^{-1} in *Rh-1U19* and 947 cm^{-1} in *Rh-1HZX*) and having the same intensity in both models with large contributions from C14H and NH waggings. It has no detectable intensity in the experimental spectrum. Finally, two normal modes calculated at 847 and 802 cm^{-1} in *Rh-1U19* (857 and 805 cm^{-1} in *Rh-1HZX*) have been assigned to C10H wag in combination with the C7=C8 B_g HOOP mode. The former mode is characterized by stronger, while the latter one by weaker C10H wag relative amplitude (Table 1). Frequencies of C10H wag in both models are only slightly affected by 10,11-^{13}C substitution (ca. 3 cm^{-1}) but downshift dramatically upon C_{10}-D substitution (ca. 125 cm^{-1}) in line with experimental data.[51]

Conclusions

In this work we have investigated how the change in the reference X-ray crystallographic structure including the relocation of a protein pocket internal water molecule may affect the vibrational properties of rhodopsin. Accordingly, the resonance Raman spectra of *Rh-1U19* and *Rh-1HZX* have been simulated by performing CASSCF/Amber vibrational frequency calculations supported by normal mode and isotopic substitution analyses.

On the basis of high-level *ab initio* calculations we managed to describe subtle changes in the vibrational structure of rhodopsin chromophore. Specifically, a significantly shorter counterion-Schiff base distance in *Rh-1U19* relative to *Rh-1HZX* manifests itself in altered vibrational frequencies and/or intensities of ethylenic, C−C bond stretching, and HOOP modes as well as frequency shift induced by N-deuteration of C=ND. Additionally, the downshifted ethylenic frequency of *Rh-1U19* is consistent with a redshift of its absorption maximum in agreement with previous studies on the electronic absorption spectra.[6]

A comparison of the most characteristic parts of the resonance Raman spectra calculated for *Rh-1HZX* and *Rh-1U19* with their experimental counterparts[8] reveals the following:

(1) The RR intensity distribution of the ethylenic band in both rhodopsin models is very similar to each other and quite similar to the experimental one. Frequencies of the vibrational modes in the C=C ethylenic band of *Rh-1U19* are in better agreement with the experimental values, e.g. the most active C=C mode is calculated at 1545 cm^{-1} for the *Rh-1U19* model, which is only 3 cm^{-1} off the experimental value, while this difference equals 8 cm^{-1} for *Rh-1HZX*.

(2) The location of the C−C vibrational modes in the fingerprint region of *Rh-1U19* more closely resembles the pattern of the measured spectrum than does the simulated spectrum based on the *Rh-1HZX* model—the frequencies of the *Rh-1U19* modes lie 4−10 cm^{-1} closer to their experimental counterparts than *Rh-1HZX* modes with the exception of the C10−C11 mode which reveals 3 cm^{-1} smaller gap between theory and experiment in case of *Rh-1HZX* model. Also, the RR intensities of C−C vibrational modes of *Rh-1U19* reveal closer agreement with the corresponding experimental intensities.

(3) The C=NH mode and its deuterated form −C=ND are calculated at frequencies that become sligthly closer (by ca. 3 cm^{-1}) to the corresponding measured values[7] in case of *Rh-1HZX* than *Rh-1U19*; however, the significantly lower deuterium shift obtained for the former model (24 cm^{-1} in *Rh-1HZX* vs 42 cm^{-1} in *Rh-1U19*) reflects the weakened Schiff base hydrogen bonding in *Rh-1HZX* as compared to the one in *Rh-1U19*.

(4) In the HOOP region observed in the 900 to 1050 cm^{-1} frequency range the relative intensity pattern of the 9-Me rock and the most active C11=C12 HOOP mode is reversed with respect to the experimental spectrum. DFT-based simulation of this spectral region, which reveals correct intensity distribution, points out to the importance of dynamic correlation effects in quantitative reproduction of the HOOP region of RR spectra of rhodopsin.[50]

Minor discrepancies between observed and calculated intensities may originate from both shortcomings of the approximate sum-overstates model, e.g. the assumption that only FC-type scattering is important and/or the neglect of the normal coordinate rotation and anharmonic effects as well as from shortcomings of the QM/MM methodology, e.g. reduced active space, lack of dynamic correlation energy, truncated basis set, lack of force field polarizibility[52] or chosen ionization status of protein residues (e.g. for Glu181).

Overall, despite the limited level of theory employed to calculate the RR spectra, our calculations do a fairly good job in reproducing the major structural features of the rhodopsin spectrum. In particular, the *Rh-1U19* model of rhodopsin seems to offer a slightly better agreement with the experimental resonance Raman spectrum[8] than *Rh-1HZX* model does.

Acknowledgment. M.O. is grateful to the Center for Photochemical Sciences and the College of Arts and Sciences for start-up funding.

Supporting Information Available: Simulated resonance Raman spectra obtained from the sum-over-states formalism and "short-time" approximation of Heller's time dependent approach. This material is available free of charge via the Internet at http://pubs.acs.org.

References

(1) Mathies, R. A.; Lugtenburg, J. In *Handbook of Biological Physics*; Stavenga, D. G., De Grip, W. J., Pugh, N. A., Jr., Eds.; Elsevier: New Amsterdam, The Netherlands, 2000; Vol. 3, pp 55−90.

(2) Palczewski, K.; Kumasaka, T.; Hori, T.; Behnke, C. A.; Motoshima, H.; Fox, B. A.; Le Trong, I.; Teller, D. C.; Okada, T.; Stenkamp, R. E.; Yamamoto, M.; Miyano, M. *Science* **2000**, *289*, 739–745.

(3) Teller, D. C.; Okada, T.; Behnke, C. A.; Palczewski, K.; Stenkamp, R. E. *Biochemistry* **2001**, *40*, 7761–7772.

(4) Okada, T.; Fujiyoshi, Y.; Silow, M.; Navaro, J.; Landau, E. M.; Shichida, Y. *Proc. Natl. Acad. Sci. U.S.A.* **2002**, *99*, 5982–5987.

(5) Okada, T.; Sugihara, M.; Bondar, A. N.; Elstner, M.; Entel, P.; Buss, V. *J. Mol. Biol.* **2004**, *342*, 571–583.

(6) Strambi, A.; Coto, P. B.; Ferré, N.; Olivucci, M. *Theor. Chem. Acc.* **2007**, *118*, 185–191.

(7) Palings, I.; Pardoen, J. A.; Van der Berg, E.; Winkel, C.; Lugtenburg, J.; Mathies, R. A. *Biochemistry* **1987**, *26*, 2544–2556.

(8) Lin, S. W.; Groesbeek, M.; van der Hoef, I.; Verdegem, P.; Lugtenburg, J.; Mathies, R. A. *J. Phys. Chem. B* **1998**, *102*, 2787–2806.

(9) Kochendoerfer, G. G.; Lin, S. W.; Sakmar, T. P.; Mathies, R. A. *Trends. Biochem. Sci.* **1999**, *24*, 300–305.

(10) Kandori, H.; Schichida, Y.; Yoshisawa, T. *Biochemistry (Moscow)* **2001**, *66*, 1197–1209.

(11) Ferré, N.; Olivucci, M. *J. Am. Chem. Soc.* **2003**, *125*, 6868–6869.

(12) Andruniów, T.; Ferré, N.; Olivucci, M. *Proc. Natl. Acad. Sci. U.S.A.* **2004**, *101*, 17908–17913.

(13) Frutos, L. M.; Andruniów, T.; Ferré, N.; Olivucci, M. *Proc. Natl. Acad. Sci. U.S.A.* **2007**, *104*, 7764–7769.

(14) Birge, R. R.; Murray, L. P.; Pierce, B. M.; Akita, H.; Baloghnair, V.; Findsen, L. A.; Nakanishi, K. *Proc. Natl. Acad. Sci. U.S.A.* **1985**, *82*, 4117–4121.

(15) Yan, E. C. Y.; Kazmi, M. A.; Ganim, Z.; Hou, J. M.; Pan, D. H.; Chang, B. S. W.; Sakmar, T. P.; Mathies, R. A. *Proc. Natl. Acad. Sci. U.S.A.* **2003**, *100*, 9262–9267.

(16) Yan, E. C. Y.; Kazmi, M. A.; De, S.; Chang, B. S. W.; Seibert, C.; Marin, E. P.; Mathies, R. A.; Sakmar, T. P. *Biochemistry* **2002**, *41*, 3620–3627.

(17) Ludeke, S.; Beck, R.; Yan, E. C. Y.; Sakmar, T. P.; Siebert, F.; Vogel, R. *J. Mol. Biol.* **2005**, *353*, 345–356.

(18) Martinez-Mayorga, K.; Pitman, M. C.; Grossfield, A.; Feller, S. E.; Brown, M. F. *J. Am. Chem. Soc.* **2006**, *128*, 16502–16503.

(19) Rohrig, U. F.; Guidoni, L.; Rothlisberger, U. *Biochemistry* **2002**, *41*, 10799–10809.

(20) Han, M.; Dedecker, B. S.; Smith, S. O. *Biophys. J.* **1993**, *65*, 899–906.

(21) Hall, K. F.; Vreven, T.; Frisch, M. J.; Beapark, M. J. *J. Mol. Biol.* **2008**, *383*, 106–121. Fahmy, K.; Jager, F.; Beck, M.; Zvyaga, T. A.; Sakmar, T. P.; Siebert, F. *Proc. Natl. Acad. Sci. U.S.A.* **1993**, *90*, 10206–10210.

(22) Cornell, W. D.; Cieplak, P.; Bayly, C. I.; Gould, I. R.; Merz, K. M., Jr.; Ferguson, D. M.; Spellmeyer, D. C.; Fox, T.; Caldwell, J. W.; Kollman, P. A. *J. Am. Chem. Soc.* **1995**, *117*, 5179–5197.

(23) Sinicropi, A.; Andruniów, T.; Ferré, N.; Basosi, R.; Olivucci, M. *J. Am. Chem. Soc.* **2005**, *127*, 11534–11535.

(24) Andruniów, T.; Fantacci, S.; De Angelis, F.; Ferré, N.; Olivucci, M. *Angew. Chem., Int. Ed.* **2005**, *44*, 6077–6081.

(25) Lumento, F.; Zanirato, V.; Fusi, S.; Busi, E.; Latterini, L.; Elisei, F.; Sinicropi, A.; Andruniów, T.; Ferré, N.; Basosi, R.; Olivucci, M. *Angew. Chem., Int. Ed.* **2007**, *46*, 412–420.

(26) Jamroz, M. H. *Vibrational Energy Distribution Analysis VEDA 4*; Warszawa, 2004.

(27) Albrecht, A. C. *J. Chem. Phys.* **1961**, *34*, 1476–1484.

(28) Manneback, C. *Physica* **1951**, *XVII*, 1001–1010.

(29) Negri, F.; Orlandi, G. Electronic and vibronic spectra of molecular systems: models and simulations based on quantum chemically computed molecular parameters. In *Computational Photochemistry*; Olivucci, M., Ed.; Elsevier: New Amsterdam, The Netherlands, 2005; Vol. 16, pp 129−169.

(30) Andruniow, T.; Pawlikowski, M. *Acta Phys. Polon.* **1996**, *93*, 707–715.

(31) Andruniow, T.; Pawlikowski, M.; Zgierski, M. Z. *J. Phys. Chem. A* **2000**, *104*, 845–851.

(32) Tonks, D. L.; Page, J. B. *Chem. Phys. Lett.* **1979**, *66*, 449–453.

(33) Blazej, D. C.; Peticolas, W. L. *J. Chem. Phys.* **1980**, *72*, 3134–3142.

(34) Chinsky, L.; Laigle, A.; Peticolas, W. L.; Turpin, P.-Y. *J. Chem. Phys.* **1982**, *76*, 1–5.

(35) Peticolas, W. L.; Rush, T., III *J. Comput. Chem.* **1995**, *16*, 1261–1270.

(36) Neugebauer, J.; Hess, B. A. *J. Chem. Phys.* **2004**, *120*, 11564–11577.

(37) Lee, S.-Y.; Heller, E. *J. Chem. Phys.* **1979**, *71*, 4777–4788.

(38) Meyers, A. B.; Mathies, R. A.; Tannor, D. J.; Heller, E. J. *J. Chem. Phys.* **1982**, *77*, 3857–3866.

(39) Myers, A. B. *J. Raman Spectrosc.* **1997**, *28*, 389–401.

(40) Frisch, M. J.; Trucks, G. W.; Schlegel, H. B.; Scuseria, G. E.; Robb, M. A.; Cheesman, J. R.; Montgomery, J. A., Jr.; Vreven, T.; Kudin, K. N.; Burant, J. C.; Millam, J. M.; Iyengar, S. S.; Tomasi, J.; Barone, V.; Mennucci, B.; Cossi, M.; Scalmani, G.; Rega, N.; Petersson, G. A.; Nakatsuji, H.; Hada, M.; Ehara, M.; Toyota, K.; Fukuda, R.; Hasegawa, J.; Ishida, M.; Nakajima, T.; Honda, Y.; Kitao, O.; Nakai, H.; Klene, M.; Li, X.; Knox, J.; Hratchian, H. P.; Cross, J. B.; Bakken, V.; Adamo, C.; Jaramillo, J.; Gomperts, R.; Stratmann, R. E.; Yazyev, O.; Austin, A. J.; Cammi, R.; Pomelli, C.; Ochterski, J. W.; Ayala, P. Y.; Morokuma, K.; Voth, G. A.; Salvador, P.; Dannenberg, J. J.; Zakrzewski, V. G.; Dapprich, S.; Daniels, A. D.; Strain, M. C.; Farkas, O.; Malick, D. K.; Rabuck, A. D.; Raghavachari, K.; Foresman, J. B.; Ortiz, J. V. Cui, Q.; Baboul, A. G.; Clifford, S.; Cioslowski, J.; Stefanov, B. B.; Liu, G.; Liashenko, A.; Piskorz, P.; Komaromi, I.; Martin, R. L.; Fox, D. J. Keith, T.; Al-Laham, M. A.; Peng, C. Y.; Nanayakkara, A.; Challacombe, M.; Gill, P. M. W.; Johnson, B.; Chen, W.; Wong, M. W.; Gonzalez, C.; People, J. A. *Gaussian03, revision C02*; Gaussian Inc.: Wallingford, CT, 2004.

(41) Ponder, J. W.; Richards, F. M. *J. Comput. Chem.* **1987**, *8*, 1016–1024.

(42) Pan, D.; Ganim, Z.; Kim, J. E.; Verhoeven, M. A.; Lugtenberg, J.; Mathies, R. A. *J. Am. Chem. Soc.* **2002**, *124*, 4857–4864.

(43) Touw, S. I. E.; De Groot, H. J. M.; Buda, F. *J. Phys. Chem. B* **2004**, *108*, 13560–13572.

(44) Aquino, A. J. A.; Barbatti, M.; Lischka, H. *ChemPhysChem* **2006**, *7*, 2089–2096.

(45) Palings, I.; Van der Berg, E. M. M.; Lugtenburg, J.; Mathies, R. A. *Biochemistry* **1989**, *28*, 1498–1507.

(46) Yan, E. C. Y.; Ganim, Z.; Kazmi, M. A.; Chang, B. S. W.; Sakmar, T. P.; Mathies, R. A. *Biochemistry* **2004**, *43*, 10867–10876.

(47) Kim, J. E.; Mc Camant, D. W.; Zhu, L.; Mathies, R. A. *J. Phys. Chem. B* **2001**, *105*, 1240–1249.

(48) Kukura, P.; Mc Camant, D. W.; Yoon, S.; Wandschneider, D. B.; Mathies, R. A. *Science* **2005**, *310*, 1006–1009.

(49) Pan, D.; Mathies, R. A. *Biochemistry* **2001**, *40*, 8557–8562.

(50) B3LYP/6-31g* Hessian calculations on the CASSCF/Amber optimized ground-state equilibrium structure. For DFT vibrational frequencies 0.97 scaling factor was employed.

(51) Eyring, G.; Curry, B.; Broek, A.; Lugtenburg, J.; Mathies, R. *Biochemistry* **1982**, *21*, 384–393.

(52) Söderhjelm, P.; Husberg, C.; Strambi, A.; Olivucci, M.; Ryde, U. *J. Chem. Theory Comput.* **2009**, *5*, 649–658.

CT900071C